Aerodynamic and thermal interference between two building models

S Korobkov, A Gnyrya and V Terekhov

[1] Construction Technology Tomsk State University of Architecture and Building, 2, Solyanaya sq., Tomsk, 634003, Russia
[2] Kutateladze Institute of Thermophysics SB RAS 1, Akademika Lavrentieva ave., Novosibirsk, 630090, Russia

Email: korobkov_1973@mail.ru

Abstract. the paper considers aerodynamic and thermal interference of separated flows between two square prisms arranged at a short distance from each other. It is shown how relative positions of the square prisms affect the specific phenomena caused by the airflow interactions. This work is the experimental study of aerodynamic and thermal interference effects on two square prisms or building models depending on their relative positions. A strong difference is shown between aerodynamic and thermal interferences observed in the airflow behind two tandem models. The thermal interference effect turns to be rather conservative as compared to the aerodynamic. Using the interference parameters one can easily analyze the extreme values of the pressure and thermal flows interfering with the building models depending on many factors, including relative model positions.

1. Introduction

In civil engineering in Russia, great attention is paid to high-rise building. The advantage of this type of buildings is a large amount of space per square meter of the site. As a result, it is possible to more compactly distribute living and working spaces in the municipal area. Building is a complex structure which unifies all design and construction solutions. In Russia, there is no yet experience in design and continuous servicing high-rise buildings as, for example, in the USA. Thus, there is broad scope for new investigations in the field of high-rise construction with regard to climatic conditions of the country.

One of the most successful methods of investigating building parameters is physical modeling. In comparison with numerical, this method is the most reliable as it completely excludes the human factor affecting the accuracy of set parameters. The significant drawback of this method is the necessity to create precise and often complex models. Moreover, this method requires purchasing large and expensive equipment.

When designing a building, it is important to be aware of many factors. Among them, wind loading is one of the most important.

It is worth noting that engineers and researchers have always shown a lot of interest in the problem of wind loading. The learning potential and technical feasibility promote opportunities to study the wind flows and their effect on different objects. The recent years are characterized by remarkable advances in the knowledge acquirement concerning the wind effect on such objects as prisms,

pyramids, cylinders, etc. In each case, the air motion has specific features. Similar methods have been used for several objects, including their mutual effect on the airflow and its turbulence.

There are two main research trends of the wind loading. The first is the wind loading on a building, which is an integral action resulting in multiple phenomena, such as static load which includes air pressure and rarefaction; dynamic load which includes airflow pulses causing vibrations of an object; and many others. Second, the air motion is a source of the convective heat exchange of a building. The latter also includes many research trends among which are heat loss and heat exchange between several objects.

Interference of separated flows is the best example of changes in the dynamic airflow and the rate of heat transfer in the studied arrangement of the building models (beyond the disturbing barrier). The interference effect allows evaluating the turbulence impact from the front barriers on the fields of pressure and heat exchange.

The literature review in the area of the airflow interference between two or more models in tandem shows that both Russian [1–4] and foreign [5–20] researches are involved in the problem. In recent years, the numerical simulation of the interference effect has become very popular [21–29]. Numerical and experimental simulation of interference of separated flows is presented, for example, in [30–32].

The results of numerous experiments on this issue achieved for the past years and their comparison with those of other authors allow highlighting general behavior of aerodynamic and thermal interference factors.

It is found that the separated flow which occurs near a group of buildings affects both the heat loss and wind loadings which, in turn, govern the internal microclimate of building, its operating parameters and safety.

Determination of the direct dependence between the heat loss and the wind pressure is still a complicated and multiple-factor problem that can be solved through the analysis and comparison of aerodynamic and thermal interference effects based on the systematic experimental studies.

This work aims at the experimental study of aerodynamic and thermal interference effects on two building models or square prisms depending on their relative positions.

2. Research Tasks. Pilot Model and Measuremet Technique

Research tasks were based on the experimental data on the wing loads and convective heat exchange. The results of multiple experiments being collected for the last few years and their comparison with those obtained by other researchers [1–32] allowed distinguishing general tendencies in the behaviour of the interference factor. At the first stage, the building models were prepared to explore the fields of pressure applied to different sides and the local and average heat transfer coefficients in the conditions of the forced convection. The second stage included the combined exploration of the wind (aerodynamic) load and thermal flows and finding common changes caused by the relative positions of the building models. Due to the large data volumes [33–35], we present the experimental results under the following conditions:

- The square prisms have the relative height H/a = 6, where a = 50 mm is the size of the cross-section.
- The square prisms are arranged on the axis of the relative airflow (Figure 1).
- The longitudinal pitch is accepted to be $L1/a$ = 0; 0.5; 1; 1.5; 3, 4.5 and 6.

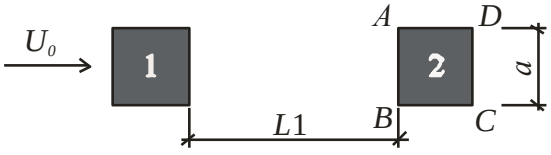

Figure 1. Plane view of building models arranged on one axis: *1* – obstruction model; *2* – model of interest. a = 50 mm; U_0 – airflow velocity; $L1$ – axial displacement.

The final data processing and the analysis of results were based on a comparison of the identical parameters. The initial parameters of the air pressure and rarefaction *Cp* and the heat transfer Nu did not allow comparing properly the changes in these parameters because of the difference in the units of measurement. On that basis, we used the interference factors IF(*Cp*) and IF(Nu) as parameters describing the rate of the aerodynamic and thermal interaction.

$$\mathrm{IF}(Cp) = \frac{Cp}{Cp_0};\ \mathrm{IF}(\mathrm{Nu}) = \frac{\mathrm{Nu}}{\mathrm{Nu}_0},$$

where *Cp* and Nu are respectively the pressure coefficient and the Nusselt number for one of the sides of the downstream Model 2; Cp_0 and Nu_0 are respectively the pressure coefficient and the Nusselt number for the whole surface of the Model 1 in front.

Figure 2 illustrates two prismatic models with the different structure for measurements of the pressure and the heat transfer coefficients. On the side of the model for the pressure measurement there are channels for the air motion that was recorded with the multichannel pressure sensor switch. A set of thermocouples was placed at the respective points on the side of the model for measuring the heat transfer coefficient.

The measurements of the static pressure and the heat transfer coefficient as well as a study of the air motion are performed on a specific aerodynamic test bench. This test bench consists of the wind tunnel, the multichannel pressure sensor switch for recording changes in the heat transfer coefficient using the downstream model and the model of interest.

The wind tunnel is an open exhausting tube, the schematic view of which is presented in Figure 3. The range of speeds in the working chamber is 1–30 m/s; the turbulent stream rate is 0.5 %. The working chamber of the wind tunnel is 1200 mm long, its cross section is 400×400 mm^2. One of the lateral sides of this chamber has two windows made of organic glass. One window is intended for the model assembling and the other is for observations and locates above the model. The chamber housing is made of steel.

The gages are placed in the working chamber via an aperture at the bottom of the channel. The aperture is sealed with a fluoroplastic band. Branch tubes are connected to the type VO–5U2 mine fan with a 7.5 kW motor. The airflow speed is varied by the speed control system using a converter. The velocity profile in the flow core is uniform; the thickness of the boundary layer at the model placement is ~20 mm frequency.

Figure 2. General view of the building model for measurements:
a – pressure, *b* – heat transfer coefficient.

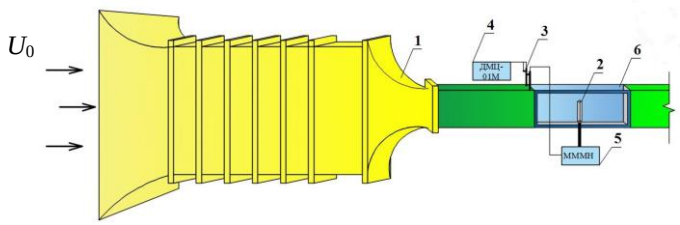

Figure 3. Schematic of the wind tunnel for static pressure measurements: *1* – wind tunnel; *2* – building models; *3* – Pitot static tube; *4* – pressure differential gage DMTs-01M; *5* – multichannel pressure sensor switch; *6* – working chamber.

Air in the wind tunnel is supplied from the outer space through the laboratory rooms. During the experiment, the air temperature is rather constant (~20°C).

A multichannel differential pressure sensor (1 mm graduation) is manufactured to vary the difference in pressure (Figure 4). The readout of information from the differential pressure sensor is provided by a digital camera, and the results are digitized in a GetData Graph Digitizer. The reference value is selected to be static pressure in the channel of the undisturbed flow.

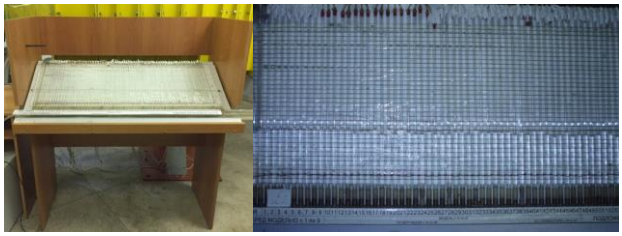

Figure 4. General view of the multichannel differential pressure sensor.

The order of calculation of the pressure coefficient *Cp* is as follows:

1. The airflow velocity U_0 is detected first:

$$U_0 = 4.429 \times \frac{\sqrt{\Delta P \times k}}{\sqrt{\rho}},$$

where ΔP is the pressure sensor readings, Pa; k is the slope coefficient; ρ is airflow density; P is the air pressure, mm Hg; $T = t_0 + 273$ is the airflow temperature, °C.

$$\rho = 0.46338 \times \frac{P}{T}$$

2. Let us define the measurement error:

a) the measurement error is the deviation from zero line (static pressure in the channel) at a 0 m/s airflow velocity. It can be detected by the difference between the sensor readings at each point of the surface and the static pressure in the channel: $h_{\text{inacc.}} = P_o - P_i$ (in mm).

b) the obtained $h_{\text{inacc.}}$ value is subtracted from $\Delta P_{inacc.} = P_o - P_i$ at the $U_0 \neq 0$.

3. Let us covert millimeters [mm] to pascals [Pa]:

$$\Delta P = h \cdot 10^{-3} \cdot g \cdot \rho,$$

where $h = n \cdot \sin(\alpha)$ is the liquid height; g is the gravity factor, m/s^2; ρ is the liquid density, kg/m^3.

4. Now we calculate the pressure coefficient:

$$C_p = \frac{p_i - p_0}{\frac{1}{2} \cdot \left(\rho \cdot U_0^2\right)},$$

where P_i is the static pressure at the *i*-th surface point, Pa; P_0 is the static pressure in the center of the channel, upstream, Pa; $1/2(\rho U_0^2)$ is the dynamic pressure of the oncoming flow; ρ is the density of the oncoming flow, kg/m^3; U_0 is the flow density, m/s.

Electric current passes through a nichrome coil to provide the surface heating in the model for the heat transfer measurements. Thermocouples were placed on one side of the model covered with a stainless steel plate 1 mm thick. The thermal boundary condition on this surface matches the stable thermal flow, i.e. q = *const*. In order to reduce the heat flow along the model, a number of slots are made as shown in Figure 2. The model is subsequently rotated to the proper angles for the heat transfer measurements on other sides.

The following equation defines the average Nusselt number for the whole surface of the model:

$$\mathrm{Nu} = \frac{\alpha \cdot a}{\lambda},$$

where α is the average heat transfer over the square model surface, W/(m^2·°C); *a* is the cross-section of the square model, m; λ is the thermal conductivity of the airflow, W/(m·°C).

As a result of these measurements, we obtained the coefficients of the pressure distribution and the heat transfer, which were used to calculate the Nusselt number. Besides mean values, the aerodynamic component of the wind loading allowed detecting the maximum and minimum values of the resulting parameters. Thus, the interference factor was calculated using not only mean but also maximum and minimum values of *Cp* and Nu.

3. Results and Discussion

At the first stage, we obtain information on the separated flow structure using the oil flow visualization of the wind tunnel surface. The results of this visualization are illustrated in Figure 5. All the models are made of organic glass 5 mm thick.

The oil flow visualization is used to detect the correlation between the obtained visible flow patterns and the distribution factor of aerodynamic and thermal interference as well as to evaluate the hydrodynamic structure of separated flows, their size and behavior.

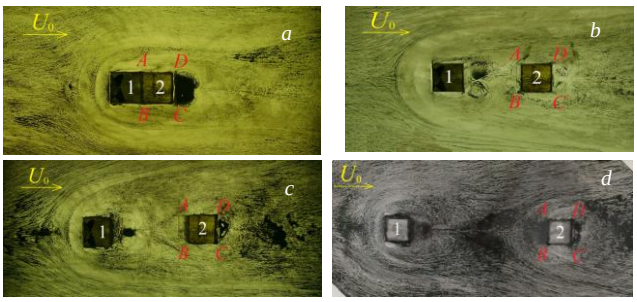

Figure 5. Oil flow visualization of the tunnel surface along two successively arranged building models.

According to Figure 5*a*, at a longitudinal pitch of $L1/a = 0$ the boundary layer is subjected to a three-dimensional separation when approximating to Model 1. The airflow structure nearby Model 1 is a horseshoe vortex which appears on the front side and extends along the lateral sides of both models, down the flow with unstable state.

The formation of vortices is observed in recirculation zones on the lateral sides. These vortices span most of the lateral sides of both models. This recirculation is unstable, periodical pulsations in the flow direction along the lateral sides of Model 1, where the inner horseshoe vortex makes U-turn.

At $L1/a = 1.5$ (Figure 5*b*), the flow recirculation notably reduces on *D*–*A* and *B*–*C* sides of Model 2. Behind Model 2 (*C*–*D* side) there is a weak contour of a dome-shape vortex. The upper side of Model 2

is in the area of the separated flow. Behind Model 1 one can see a dome-shape vortex which occupies most of the space between the models.

At $L1/a$ = 3.0 (Figure 5*c*), the area occupied by the dome-shape vortex increases between the models by almost two times. The flow recirculation on *D–A* and *B–C* sides continues to reduce. The dome-shape vortex behind Model 2 (*C–D* side) becomes well-defined but less intensive than the similar vortex generated by Model 1. The rest of the flow parameters on *A–B* side and upper sides of Model 2 stay unchanged.

At $L1/a$ = 6.0 (Figure 5*d*), a contour of the dome-shape vortex appears on the front A–B side of Model 2, which then propagates onto the lateral sides *D–A* and *B–C*. The flow separates from Model 1 and attaches to the upper side of Model 2. The impact of the dome-like vortex on Model 2 decreases. Recirculation zones are not observed on the lateral sides *D–A* and *B–C*. Such an arrangement levels the influence of the front model. And a further increase in the distance between the models allows considering Model 2 as a freestanding.

Let us now discuss aerodynamic and thermal interference in the system of two building models.

Firstly, the effective analysis is necessary for grouping the diagrams by the model sides and types of measurements (aerodynamic and thermal). Secondly, the individual analysis of medium, maximum and minimum values is required. Thirdly, the mutual analysis should be conducted for aerodynamic and thermal interference depending on the distance $L1/a$ between the wind tunnel models at the airflow angle of attack. Let us discuss the results obtained.

According to Figure 6, the aerodynamic interference factor on the front side *A–B* of Model 2 strongly depends on the relative position of the models (Figure 6*a*). The interference factor is higher for the lowest values of the pressure coefficient *Cp* than for the mean (integrated) or maximum values. This is because the air rarefaction enabled by the model in front. The highest interference factor is observed at a relative distance $L1/a$ = 4.5, when the measuring model is exposed to the horseshoe vortex.

Unlike aerodynamic, thermal interference effect shown in Figure 6*b* is less dependent on the distance $L1/a$ between the models. At the same time, their mean, maximum and minimum values do not significantly differ from one another. The highest values of IF(Nu) are observed for the integrated value of the interference factor. The effect of aerodynamic interference observed along the sides *B–C* and *D–A* of Model 2 (Figure 7*a*) is higher at $L1/a$ = 0.5…3. This is caused by the accelerated airflow along the sides of Model 2. At $L1/a$ = 3…∞ this effect is lower.

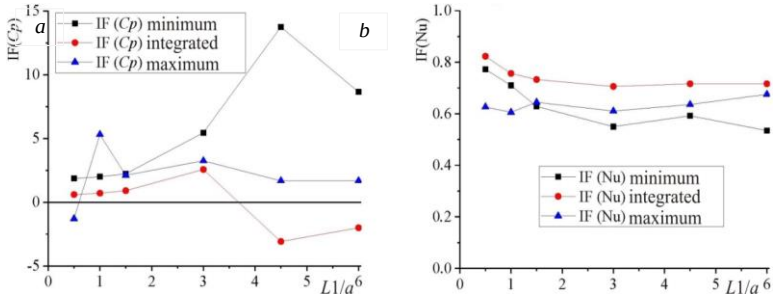

Figure 6. Distribution factor of aerodynamic (a) and thermal (b) interferences along the side A–B of Model.

The thermal interference effect in Figure 7*b* continues to be constant at all values of $L1/a$. The maximum IF(Nu) values match the integrated values in most cases.

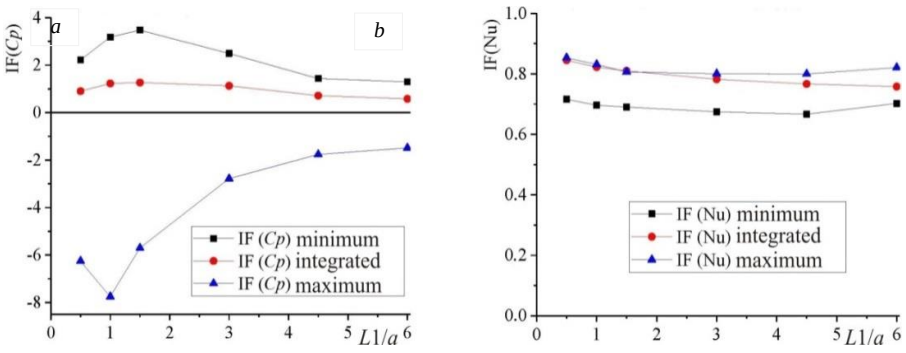

Figure 7. Distribution factor of aerodynamic (*a*) and thermal (*b*) interferences along sides *B*–*C* and *D*–*A* of Model 2.

According to Figure 8, the interference effect on the back side *C*–*D* of Model 2 is less dependent on *L*1/*a* distance and seems not to be significantly changed. It should be only mentioned that interference changes at *L*1/*a* = 1.5 (Figure 8*a*), when the vortex zone formed by the front Model 1 affects the side of Model 2 and is strengthened by the separated flows from edges *B* and *A*.

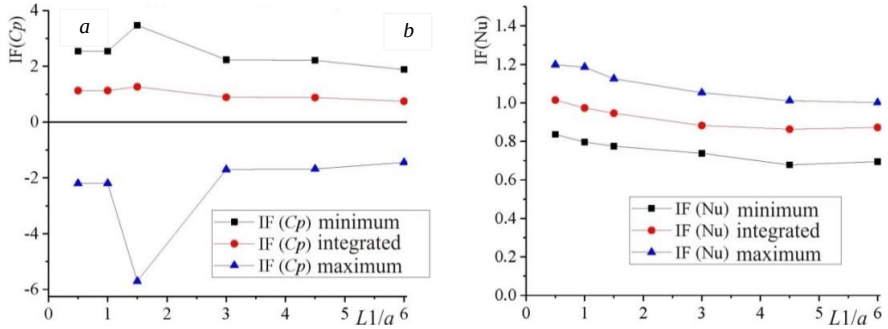

Figure 8. Distribution factor of aerodynamic (a) and thermal (b) interferences along the back side *C*–*D* of Model 2.

4. Conclusion

This study showed that the factors of aerodynamic and thermal interferences observed beyond the disturbing building model differed strongly. The thermal interference effect was rather conservative as compared to the aerodynamic. The highest values of the thermal interference effect were observed on the back side *C*–*D* in the vortex zone beyond the model.

Based on the description of aerodynamic and thermal interference effects it can be concluded that aerodynamic interference is more subjected to changes depending on the distance between the building models, i.e. at *L*1/*a* > 3 the changes occurred on *A*–*B* side, and at *L*1/*a* < 3 they were observed on other sides.

Using the interference parameters one can easily analyze the extreme values of the pressure and thermal flows on the model surfaces depending on many factors, including their relative positions.

5. Acknowledgement

This work was carried out within the state contract N AAAA-A17-117030310010-9 and financially supported by Grant N 18-08-01025 from the Russian Foundation for Basic Research.

References

[1] Salenko S D, Obukhovskii A D, Gosteev Yu A and Telkova Yu V 2010 Flow structure investigation around two square cross-section beams under interference conditions *Thermophys. Aeromech.* **17** 291–300
[2] Salenko S D, Odnopal V P, Obukhovskii A D, Gosteev Yu A and Telkova Yu V 2010 Aerodynamic studies of high-rise building complex *ABOK* **5** 62–66
[3] Guzeyev A S, Kornilov D V, Korotkin A I and Solov'ev S Yu 2015 Aerodynamic tests of high-rise buildings *Tall Buildings* **1** 102
[4] Guzeev A S, Korotkin A I, Lebedev A O and Rogovoi Yu A 2009 Analysis of some results in determining the aerodynamic characteristics of multistorey building *Magaz. Civil Eng.* **3(5)** 50–52
[5] Kim W, Tamura Y and Yoshida A2015 Interference effects on local peak pressures between two buildings *J. Wind Eng. Ind. Aerod.* **147** 186–201
[6] Yu X F, Xie Z N, Zhu J B and Gu M 2015 Interference effects on wind pressure distribution between two high-rise buildings *J. Wind Eng. Ind. Aerod.* **142** 188–97
[7] Yu X F, Xie Z N, Wang X and Ca B 2016 Interference effects between two high-rise buildings on wind-induced torsion *J. Wind Eng. Ind. Aerod.* **159** 123–33
[8] Yu X F, Xie Z N, and Gu M 2018 Interference effects between two tall buildings with different section sizes on wind-induced acceleration *J. Wind Eng. Ind. Aerod.* **182** 16–26
[9] Hui Y, Yoshida A and Tamura Y 2013 Interference effects between two rectangular-section high-rise buildings on local peak pressure coefficients *J. Fluids and Structures* **37** 120–33
[10] Hui Y, Tamura Y and Q S Yang Q S 2017 Analysis of interference effects on torsional moment between two high-rise buildings based on pressure and flow field measurement *J. Wind Eng. Ind. Aerod.* 164 54–68
[11] J A Amin J A and A Ahuja A 2012 Wind-induced mean interference effects between two closed spaced buildings *J. Civil Engineering* **16** 119–31
[12] Gu M and Xie Z N 2011 Interference effects of two and three super-tall buildings under wind action *J. Acta. Mech. Sin.* **1 (27)** 687–96
[13] Lam K M, Zhao J G and Leung M Y H 2011 Wind-induced loading and dynamic responses of a row of tall buildingsunder strong interference *J. Wind Eng. Ind. Aerod.* **99** 573–83
[14] Zu G B and Lam K M 2018 Across-wind excitation mechanism for interference of twin tall buildings in staggered arrangement *J. Wind Eng. Ind. Aerod.* **177** 167–85
[15] Huang D, Zhu L, Ding Q, Zhu X and Chen W 2017 Aeroelastic and aerodynamic interference effects on a high-rise building *J. Fluids and Structures* **69** 355–81
[16] Mara T G, Terry B K, Ho T C E and Isyumov N 2014 Aerodynamic and peak response interference factors for an upstream square building of identical height *J. Wind Eng. Ind. Aerod.* **133** 200–10
[17] Wonsul K, Yukio T and Akihito Y 2015 Interference effects on aerodynamic wind forces between two buildings " *J. Wind Eng. Ind. Aerod.* **147** 186–201
[18] Flaga A, Koco A, Kłaput R and Bosak G 2018 The environmental effects of aerodynamic interference between two closely positioned irregular high buildings *J. Wind Eng. Ind. Aerod.* **180** 276–87
[19] Pundhir R and Barde N 2016 Study of wind pressure on tall building due to change in relative position of interfering building *Int. J. Civil Eng. Research* **7** 105–15
[20] Lau S C, Cervantes J, Han J C, Rudolph R J and Flannery K 2003 Measurements of wall heat (mass) transfer for flow through blockages with round and square holes in a wide rectangular channel *Int. J. Heat Mass Tran.* **46** 3991–401
[21] Bairagi A K and Dalui S K 2014 Optimization of interference effects on high-rise buildings for different wind angle using CFD simulation *Electron J. Struct. Eng.* **14** 39–49
[22] Lankadasu A and Vengadesan S 2008 Interference effect of two equal-sized square cylinders in tandem arrangement: with planar shear flow *Int. J. Numer. Methods Fluids* **57** 1005–21

[23] Qu Y, Milliez M, Musson-Genon L and Carissimo B 2012 Numerical study of the thermal effects of buildings on low-speed airflow taking into account 3D atmospheric radiation in urban canopy *J. Wind Eng. Ind. Aerod.* **104–106** 474–83
[24] Martinuzzi R, AbuOmar M and Savory E 2007 Scaling of the wall pressure field around surface-mounted pyramids and other bluff bodies *J. Fluids Eng.* 129 1147–56
[25] Val'ger S A, Fedorov A V and Federova N N 2013 Modeling of incompressible turbulent flows in the vicinity of poorly streamlined bodies using ANSYS Fluent *Computational Technologies* **18** (5) 27–40
[26] Isaev S A, Baranov P A, Zhukova Yu V, Tereshkin A A and Usachov A E 2014 Simulation of the wind effect on an ensemble of high-rise buildings by means of multiblock computational technologies *J. Eng. Phys. and Thermophys.* **87** 112–123
[27] Isaev S A, Vatin N I, Lebiga V A, Zinoviev V N, Chang K –C and Miau J –J 2013 Problems and methods of numerical and experimental investigation of high rise constructions' aerodynamics in the coastal region 'sea-land' *Magaz. Civil Eng.* **2** 54–61
[28] Belostotskii A M, Dubinskii S I and Afanas'eva I N 2010 Numerical modeling of building aerodynamics problems Development of methods and research of real objects *I.Journal of Civil and Structural Engineering* **6** 67–69
[29] Guvernyuk S V, Sinyavin A A and Gagarin V G 2019 Rapid assessment of integrated wind loads on high-rise building *Zhilishchnoe stroitel'stvo* **6** 43–48
[30] Covak L, Öztürk E, Balci M N and Körpe S B 2010 Numerical and experimental analysis of wind loads on cladding of tall buildings *Proceedings of the 7th international conference Heat transfer fluid mechanics and thermodynamics* 1709–1714 (Antalya, Turkey)
[31] Pillai S S and Yoshie R 2012 Experimental and numerical studies on convective heat transfer from various urban canopy configurations *J. Wind Eng. Ind. Aerod.* **104–106** 447–54
[32] Guvernyuk S V, Egorychev O O, Isaev S A, Kornev N V and Poddaeva O I 2011 Numerical and physical simulation of wind load on a group of high-rise buildings *Vestnik MGSU* **3–1** 185–191
[33] Koshin A A, Korobkov S V, Gnyrya A I and Terekhov V I 2017 Modeling of vortex structure and wind load at nonlinear arrangement of two square prisms *Proceedings of all-Russian conference XXXI Siberian thermal physics seminar devoted to the 100th birthday of Academician Kutateladze* 389–392 (IT SB RAS Novosibirsk Russia)
[34] Mokshin D I 2015 *Convective Heat Exchaingle of Single and Tandem-Arranged Models* PhD Thesis (Tomsk: Tomsk State University of Architecture and Building)
[35] Gnyria A, Korobkov S, Koshin A and Terekhov V 2017 Aerodynamic and thermal interference of turbulent separated flows over building models *MATEC Web Conf* **115** 1–4